Controlling Grain Boundaries by Magnetic Fields

R. Backofen,[1] K. R. Elder,[2] and A. Voigt[1,3]
[1]Institute of Scientific Computing, Technische Universität Dresden, 01062 Dresden, Germany
[2]Department of Physics, Oakland University, Rochester, Michigan 48309, USA
[3]Dresden Center for Computational Materials Science (DCMS), 01062 Dresden, Germany

(Received 20 November 2018; published 29 March 2019)

The ability to use external magnetic fields to influence the microstructure in polycrystalline materials has potential applications in microstructural engineering. To explore this potential and to understand the complex interactions between electromagnetic fields and solid-state matter transport we consider a phase-field-crystal model. Together with efficient and scalable numerical algorithms this allows the examination of the role that external magnetic fields play on the evolution of defect structures and grain boundaries, on diffusive timescales. Examples for planar and circular grain boundaries explain the essential atomistic processes and large scale simulations in 2D are used to obtain statistical data on grain growth under the influence of external fields.

DOI: 10.1103/PhysRevLett.122.126103

It is well known that material properties of polycrystalline materials are strongly influenced by the average grain size. For example, in some compounds the magnetic coercivity can increase by orders of magnitude as the grain size changes from nanoscales to micron scales [1–4]. In metals, the yield strength can not only change dramatically with grain size (the so-called Hall-Petch effect [5–10]) but it is also influenced by details of the grain size distribution [11]. Each of the cases highlights the importance of the grain structure and the technological need to understand and control its formation.

The use of external magnetic fields offers additional degrees of freedom to synthesize materials and to tailor the grain structure and thus material properties. Although evidence for the interactions between external magnetic fields, diffusion, and irreversible deformation mechanisms has been gathered over the years, see the review [12], a global yet detailed understanding of the interactions between magnetic fields and solid-state matter transport is far from being reached. In this Letter, we analyze the properties of a theoretical model, which allows the description of the basic physics of magnetocrystalline interactions in a multiscale approach, combining the dynamics of defects, dislocation networks, and grain boundaries with experimentally accessible microstructure evolution on diffusive timescales.

The basic mechanisms of this interaction can be understood on thermodynamic arguments. In magnetic materials the magnetic moments are aligned with a sufficiently strong external magnetic field. If the magnetic properties of the material are anisotropic, the bulk free energy differs for differently oriented grains and the energy difference can influence grain boundary (GB) movement. The dynamics of the GB can be described by Mullins-type models [13]

$$v = -M(\gamma\kappa - \Delta f) \tag{1}$$

extended by the bulk energy difference [14,15], where v is the normal velocity of the GB, M a mobility function, κ the mean curvature, and Δf the energy density difference of the grains. Assuming two differently oriented grains in a strong magnetic field in a circular and planar setting, see Supplemental Material for details [16], the total energy of the system and (1) lead to a critical grain size $r_c = -\gamma/\Delta f$ in the circular and a constant $v \propto \Delta f$ in the planar setting. Both cases demonstrate the possibility to influence GB movement by external magnetic fields. However, the description ignores the underlying crystalline lattice which can influence the process.

It has been shown that the complex dislocation structure along curved GB gives rise to a misorientation-dependent mobility [19]. Further studies indicate that grain boundaries undergo thermal roughening associated with an abrupt mobility change, leading to smooth (fast) and rough (slow) boundaries [20], which can eventually lead to stagnation of the growth process. The defect structure at triple junctions can lead to a sufficiently small mobility limiting the rate of GB migration [21,22]. Also, tangential motion of the lattices is possible. For low-angle GB, normal and tangential motion are strongly coupled as a result of the geometric constraint that the lattices of two crystals change continuously across the interface while the GB moves [23]. As a consequence of this coupling, grains rotate as they shrink, which leads to an increase in the GB energy per unit length, although the overall energy decreases since the size of the boundary decreases [24–28].

The phase field crystal (PFC) model [29–32], captures all these complex features and numerical simulations of the model have been shown to recover the characteristic grain size distribution in agreement with detailed experimental results [33]. Numerous publications have shown the model

to capture the essential physics of atomic-scale elastic and plastic effects that accompany diffusive phase transformations, such as solidification, dislocation kinetics, and solid-state precipitation, see [34] for a review.

In [35] the model is coupled with magnetization to generate a ferromagnetic solid below a density-dependent Curie temperature. In [36] this model is extended and used to demonstrate the influence of magnetic fields on the growth of crystal grains. These results indicate that a greater portion of grains evolve to become aligned along the easy direction of the crystal structure with respect to the orientation of the external magnetic field. In this Letter, we use it to predict the influence of the magnetic field on grain coarsening in polycrystals. Consistent with the thermodynamic arguments we find that when the magnetic field is applied, the average grain size increases and the number of grains along the easy direction with respect to the field increases. However, it is also found that the grains become elongated when the field is applied. The elongation occurs due to an anisotropic GB mobility in the presence of an applied field.

The model in [35,36] combines the rescaled number density φ with a mean field approximation for the averaged magnetization $\mathbf{m}$. The energy $\mathcal{F}[\varphi,\mathbf{m}] = \int f_{\mathrm{PFC}}[\varphi] + \omega_B f_m[\mathbf{m}] + \omega_B f_c[\varphi,\mathbf{m}]d\mathbf{r}$ with

$$f_{\mathrm{PFC}}[\varphi] = \frac{1}{2}\varphi[\mathbf{r}]^2 - \frac{t}{6}\varphi[\mathbf{r}]^3 + \frac{v}{12}\varphi[\mathbf{r}]^4 - \frac{1}{2}\varphi[\mathbf{r}]\int C_2(\mathbf{r}-\mathbf{r}')\varphi[\mathbf{r}']d\mathbf{r}'$$

$$f_m[\mathbf{m}] = \frac{W_0^2}{2}(\nabla\cdot\mathbf{m})^2 + r_m\frac{\mathbf{m}^2}{2} + \gamma_m\frac{\mathbf{m}^4}{4} - \mathbf{m}\cdot\mathbf{B} + \frac{\mathbf{B}^2}{2}$$

$$f_c[\varphi,\mathbf{m}] = -\omega_m\varphi^2\frac{\mathbf{m}^2}{2} - \sum_{j=1}^{2}\frac{\alpha_{2j}}{2j}(\mathbf{m}\cdot\nabla\varphi)^{2j},$$

consists of contributions related to local ordering of the crystal, to local orientation of the magnetic moment and to coupling between crystal structure and magnetization. ω_B is a parameter to control the influence of the magnetic energy. In order to maximize the anisotropy in the 2D setting, a square ordering of the crystal is preferred, which is realized within the structural PFC formulation for $f_{\mathrm{PFC}}[\varphi]$, see [37,38] and Supplemental Material [16].

Magnetization in an isotropic and homogenous material is modeled by $f_m[\mathbf{m}]$. The first three terms define a mean field theory of a vector field which is minimized by $|\mathbf{m}|=0$ for $r_m>0$ and $|\mathbf{m}|=-r_m/\gamma_m$ for $r_m<0$. Thus, a negative r_m leads to ferromagnetic properties. The last two terms describe the interaction of the magnetization with an external and a self-induced magnetic field, $\mathbf{B}_{\mathrm{ext}}$ and $\mathbf{B}_{\mathrm{ind}}$, respectively. The magnetic field is defined as $\mathbf{B}=\mathbf{B}_{\mathrm{ext}}+\mathbf{B}_{\mathrm{ind}}$, where $\mathbf{B}_{\mathrm{ind}}$ is defined with help of the vector potential: $\mathbf{B}_{\mathrm{ind}} = \nabla\times\mathbf{A}$ and $\nabla^2\mathbf{A} = -\nabla\times\mathbf{m}$.

The magnetic anisotropy of the material is due to the crystalline structure of the material. Thus, the magnetization has to depend on the local structure represented by φ and vice versa. The first term in $f_c[\varphi,\mathbf{m}]$, changes the ferromagnetic transition in the magnetic free energy. On average, φ^2 is larger in the crystal than in the homogeneous phase. Thus, ω_m and r_m can be chosen to realize a paramagnetic homogeneous phase and a ferromagnetic crystal. The second term depends on average on the relative orientation of the crystalline structure with respect to the magnetization. In our case, it leads to an energetic minimum if the magnetization is aligned with the diagonal of the square crystal. The number density φ evolves according to conserved dynamics and magnetization according to nonconserved dynamics,

$$\frac{\partial\varphi}{\partial t} = M_n\nabla^2\frac{\delta\mathcal{F}[\varphi,\mathbf{m}]}{\delta\varphi}, \qquad \frac{\partial m_i}{\partial t} = -M_m\frac{\delta\mathcal{F}[\varphi,\mathbf{m}]}{\delta m_i} \tag{2}$$

$i=1,\ 2$, respectively. See Supplemental Material for details [16].

To measure the magnetic anisotropy we consider a single crystal and vary $\mathbf{B}_{\mathrm{ext}}$. The simulation domain perfectly fits the equilibrium crystal for $\omega_B = 0$ and is small enough to prevent the appearance of magnetic domains. The parameters are chosen for a ferromagnetic material, see Supplemental Material for details [16]. Figure 1 shows the anisotropy of the bulk free energy with respect to the orientation of the magnetic moments with and without an external magnetic field. Restricting the magnetic moments to the direction of the external magnetic field, leads to slightly larger bulk energies for orientations not along hard and easy direction. This is due to the reduced degrees of freedom for energy

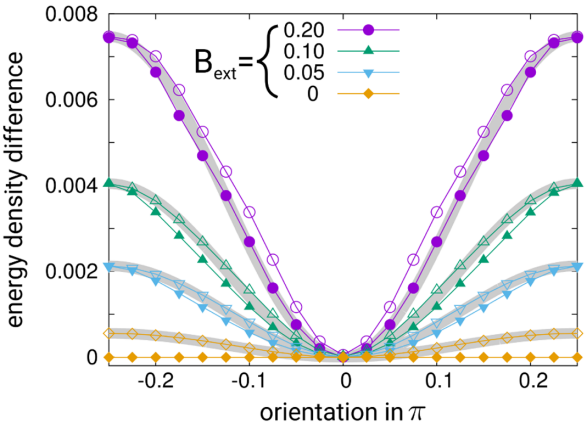

FIG. 1. Energy density deviation in a single crystal induced by $\mathbf{B}_{\mathrm{ext}}$ and measured relative to a crystal preferably aligned with $\mathbf{B}_{\mathrm{ext}}$. The orientation with respect to the crystal structure and strength of $\mathbf{B}_{\mathrm{ext}}$ is varied. Open symbols correspond to forced alignment of magnetic moments with $\mathbf{B}_{\mathrm{ext}}$, closed symbols show computed magnetic moments, gray curves show fits by cosine functions.

minimization and shows that in the full model in these cases the magnetic moments are not perfectly aligned with $\mathbf{B}_{\text{ext}}$. However, the differences are small. The magnetic anisotropy for both cases follows the fourfold symmetry of the crystal and the easy directions are along the $\langle 1\,1 \rangle$ directions. Increasing $\mathbf{B}_{\text{ext}}$ increases the anisotropy as well as the mean magnetization. The model also includes magnetostriction effects [35]. The crystal slightly tends to elongate along the easy direction aligned with $\mathbf{B}_{\text{ext}}$, see Supplemental Material for details [16].

To show the impact of external magnetic fields on the texture evolution during coarsening we prepared a polycrystalline sample, see Fig. 2. An initially randomly perturbated density field is evolved without magnetic interaction until the fine polycrystalline structure appears. Any particle with four neighbors is identified as a particle in a crystalline structure and the local orientation of the crystal with respect to the external magnetic field is calculated and visualized. Starting from this initial condition the evolution equations are solved with small random magnetization for different external magnetic fields, applied in x direction. For $B_{\text{ext}} = 0$ there is no energetically preferred orientation and coarsening is only due to minimization of GB energy. Small grains vanish and larger grains grow. The average grain size increases and the orientation distribution stays isotropic. Applying an external field leads to a preferred growth of grains which are aligned preferably with respect to the external magnetic field, the easy direction (green). Thus, the not aligned grains (blue and red) vanish and the orientation distribution peaks near the aligned grain orientation. This is in qualitative agreement with experiments, e.g., on Zn and Ti sheets [39], and classical grain growth simulations of Mullins type with an analytical magnetic driving force [40]. The additional driving force, due to the external magnetic field, also enhances the coarsening process, which can already be seen by comparing the final textures in Fig. 2 and which has also been observed experimentally, e.g., during annealing of FeCo under high steady magnetic fields [41]. Increasing $\mathbf{B}_{\text{ext}}$ leads to more pronounced grain orientation selection. For further quantification of these effects, see Supplemental Material [16].

In order to analyze these results in more detail we consider the two settings of a circular and a planar GB, see Supplemental Material [16]. We start with a rotated crystal embedded in a matrix, see Fig. 3. For $B_{\text{ext}} = 0$ the grain shrinks and vanishes in order to minimize GB energy. $\mathbf{B}_{\text{ext}}$ aligned with the easy direction of the rotated grain induces an opposite driving force, which for $B_{\text{ext}} = 0.1$ balances the GB energy, while increasing $\mathbf{B}_{\text{ext}}$ above this threshold leads

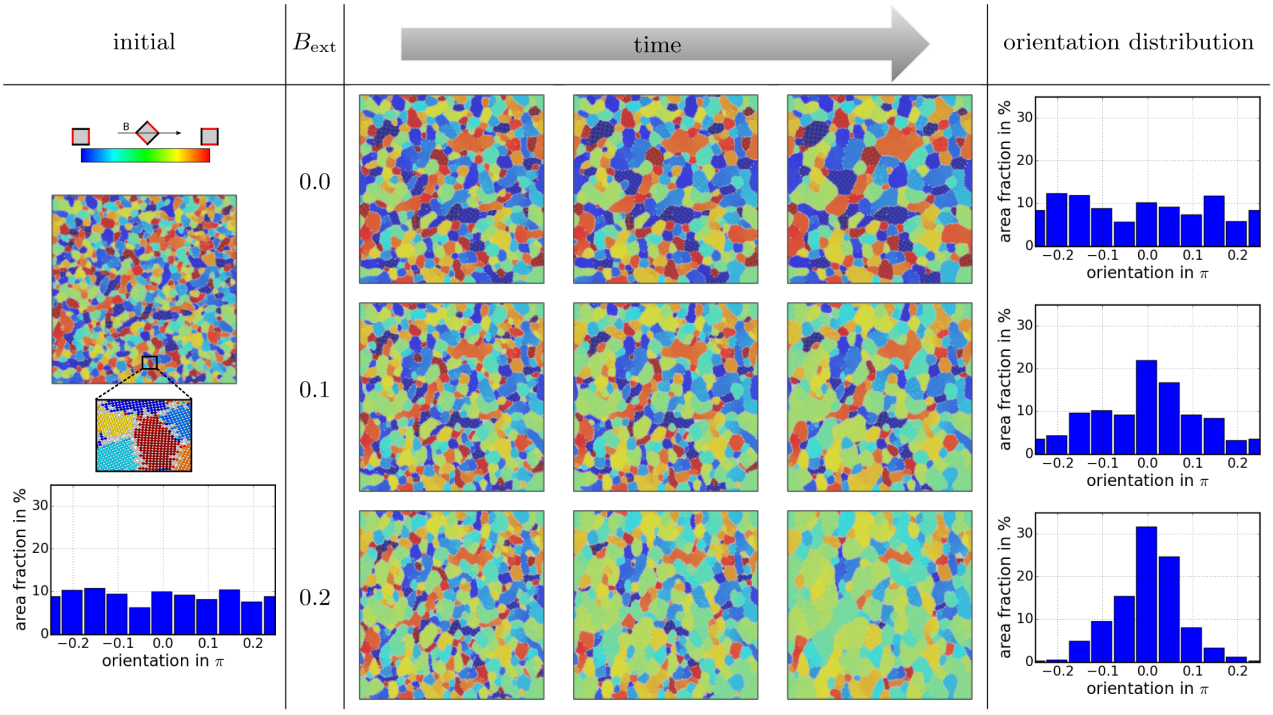

FIG. 2. (left) Initial configuration for coarsening simulation. The color shows the local orientation of the crystal with respect to the external magnetic field. The direction of the external magnetic field is in the x direction and corresponds to grains oriented in the easy direction (green). For the inlet the maxima of φ are visualized as atoms. The orientation distribution is isotropic. (middle) Coarsening simulation for different $\mathbf{B}_{\text{ext}}$ (up-down) with snapshots in time (left-right). (right) Orientation distribution at final time of coarsening process. For the used parameters, see Supplemental Material [16]. The computational domain is 409.6×409.6.

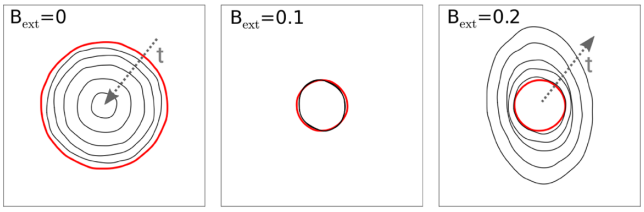

FIG. 3. A circular grain embedded in a matrix (red isoline). The external magnetic filed is aligned with the easy direction of the circular grain. Dependent on the strength of $\mathbf{B}_{\text{ext}}$ the grain shrinks, stagnates, or grows, see Supplemental Material for details [16].

to growth of the grain. This is in accordance with the continuous description.

However, for $B_{\text{ext}} = 0.2$ the evolution is anisotropic; first a squarelike shape is reached, resampling the fourfold crystalline symmetry, while further growth breaks this symmetry, the grain becomes elongated perpendicular to $\mathbf{B}_{\text{ext}}$. This may be explained by thermodynamic or kinetic reasons [42,43]. Within the continuous description of Eq. (1) the shape reached for $B_{\text{ext}} = 0.2$ requires either the GB energy γ parallel to $\mathbf{B}_{\text{ext}}$ to be roughly twice the energy perpendicular to $\mathbf{B}_{\text{ext}}$ or the mobility M of parallel and perpendicular GB has to vary by a factor of 2 or some combination of both.

To separate thermodynamic (γ) and kinetic effects (M) of GB movement, we consider a planar GB. According to the continuum description the velocity of the planar GB is proportional to the driving force Δf. Thus, the decay of total energy is linear and the mobility can be extracted, $M = -v/\Delta f$. To maximize the influence of $\mathbf{B}_{\text{ext}}$ two symmetric high angle GB are placed in an elongated periodic domain. $\mathbf{B}_{\text{ext}}$ is aligned with the easy direction of the left grain. Because of symmetry the magnetic field can be rotated by $\pi/2$. In one situation the magnetization is more aligned and in the other more perpendicular to the GB, see Fig. 4, which shows the setup and the energy decay for both situations. The initial condition is achieved

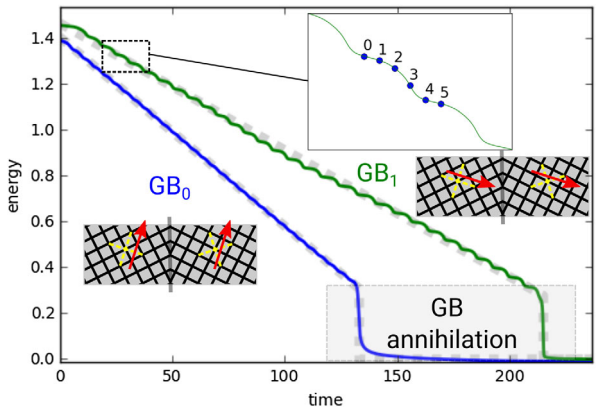

FIG. 4. Two setups of a symmetric tilt GB in a periodic domain, $B_{\text{ext}} = 0.1$ is aligned with the easy directions of the left grain. Both setups lead to the same driving force, but the energy decay differs.

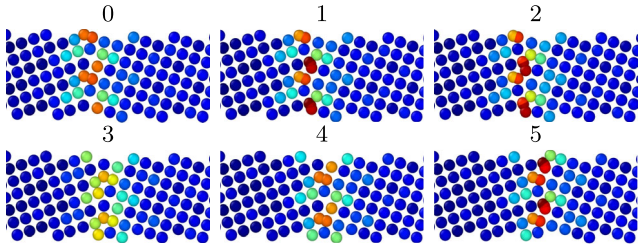

FIG. 5. Particle picture of the GB during evolution over one unit length. The particles are located according to maxima in the density field φ. The color is the energy density at the position of the particle and serves as a measure of the local energy, see [45]. During the slow evolution (0–2) the energy of the particles at the GB increases until the energy barrier is overcome by the magnetic driving force leading to a speed up of the GB and a decrease of the energy at the GB (2–3), before the next barrier is reached (3–4) and the energy at the GB increases again (4–5).

by a purely structural relaxation with $\omega_B = 0$. Then the coupling with $\mathbf{B}_{\text{ext}}$ is switched on. After some initial reconfiguration, which adjusts the density field φ, the energy decays on average linearly. The GBs move with constant speed reducing the size of the grain not aligned with $\mathbf{B}_{\text{ext}}$ until they vanish. The final annihilation of the GB leads to a sudden drop in energy, which is proportional to γ and equal in both cases. However, the energy decays faster in the case of a more aligned $\mathbf{B}_{\text{ext}}$ with the GB, implying faster GB velocity and in turn a larger GB mobility.

A closer look at the energy decay shows a steplike function. This reflects the crystalline structure of the GB. In order to move the GB by a unit length it has to pass some energetically unfavorable positions, see Fig. 5 and Supplemental Material for details [16]. Varying the magnitude of $\mathbf{B}_{\text{ext}}$ changes the driving force and the velocity of

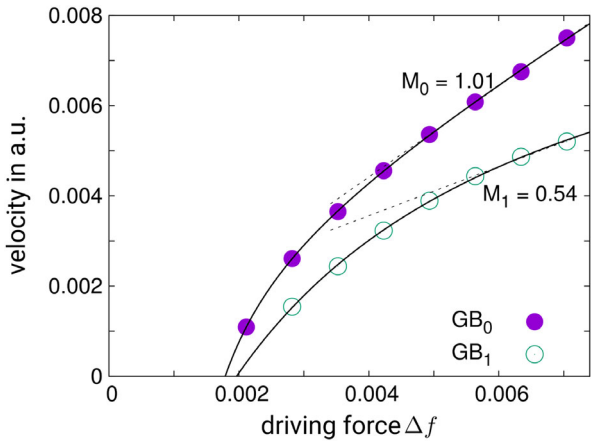

FIG. 6. Velocity extracted for the setups defined in Fig. 4. For small external magnetic field the GB is pinned and does not move at all. High driving forces lead to a linear increase of velocity with Δf and an assumed mobility becomes constant. The mobility differs by a factor of 2.

the GB, see Fig. 6. For large driving forces the dependency of the velocity is linear for both cases but by a factor 2 smaller for the case of $\mathbf{B}_{\mathrm{ext}}$ more perpendicular to the GB. For driving forces below a threshold the GB does not move, indicating the presence of an activation barrier, which has also been measured experimentally for planar GB in Zn bicrystals [44]. For intermediate regimes the mobility increases. As a consequence, the anisotropy seen in Fig. 3 can be attributed to kinetics and not thermodynamic effects, which was also claimed in [39] by interpreting the experiments on Zn and Ti.

In summary, we have shown that an applied magnetic field can increase the coarsening rate in grain growth processes, due to the lower energy of grains with their easy axis in line with the applied field. We have also shown that the mobility of GB is anisotropic with respect to the applied magnetic field. This kinetic effect leads to elongated grains. Both of these influences are intimately related to the magnetically anisotropic nature of the model studied. That is, the crystal reacts elastically on applied magnetic fields (magnetorestriction) and additionally changes in the density field reflecting the twofold symmetry of $\mathbf{B}_{\mathrm{ext}}$ may lead to preferred diffusion path and, thus, influence the mobility. It should be noted that the study examined the influence of an applied field on a ferromagnetic nanocrystalline system and did not examine the influence of magnetic field on the initial nucleation stage. This is left for future study.

A. V. and R. B. acknowledge support by the German Research Foundation (DFG) under Grant No. Vo899/19-1 in SPP1959. We further acknowledge computing resources provided at Jülich Supercomputing Center under Grant No. HDR06.

[1] G. Herzer, Acta Mater. **61**, 718 (2013).
[2] C. H. Chen, S. Kodat, M. H. Walmer, S.-F. Chen, M. A. Willard, and V. G. Harris, J. Appl. Phys. **93**, 7966 (2003).
[3] S. Roy, I. Dubenko, D. D. Edorh, and N. Ali, J. Appl. Phys. **96**, 1202 (2004).
[4] D. Xue, G. Chai, X. Li, and X. Fan, J. Magn. Magn. Mater. **320**, 1541 (2008).
[5] S. Yip, Nature (London) **391**, 532 (1998).
[6] E. O. Hall, Proc. Phys. Soc. London Sect. B **64**, 747 (1951).
[7] N. J. Petch, J. Iron Steel Inst., London **174**, 25 (1953).
[8] A. Cracknell and N. Petch, Acta Metall. **3**, 186 (1955).
[9] K. Lu, W. Wei, and J. Wang, Scr. Metall. Mater. **24**, 2319 (1990).
[10] A. Chokshi, A. Rosen, J. Karch, and H. Gleiter, Scr. Metall. **23**, 1679 (1989).
[11] C. F. Dahlberg and J. Faleskog, Eur. J. Mech. A **44**, 1 (2014).
[12] O. Guillon, C. Elsässer, O. Gutfleisch, J. Janek, S. Korte-Kerzel, D. Raabe, and C. Volkert, Mater. Today **21**, 527 (2018).
[13] W. Mullins, J. Appl. Phys. **27**, 900 (1956).
[14] S. Angenent and M. E. Gurtin, Arch. Ration. Mech. Anal. **108**, 323 (1989).
[15] J. E. Taylor and J. W. Cahn, J. Stat. Phys. **77**, 183 (1994).
[16] See Supplemental Material at http://link.aps.org/supplemental/10.1103/PhysRevLett.122.126103 for details of the numerical approach, set up and evaluation of simulations, which includes Refs. [17,18].
[17] R. Backofen, A. Rätz, and A. Voigt, Philos. Mag. Lett. **87**, 813 (2007).
[18] S. Praetorius and A. Voigt, SIAM J. Sci. Comput. **37**, B425 (2015).
[19] M. Winning, G. Gottstein, and L. Shvindlerman, Acta Mater. **49**, 211 (2001).
[20] E. Holm and S. Foiles, Science **328**, 1138 (2010).
[21] S. Srinivasan, J. Cahn, H. Jonsson, and G. Kalonji, Acta Mater. **47**, 2821 (1999).
[22] M. Upmanyu, D. Srolovitz, L. Shvindlerman, and G. Gottstein, Acta Mater. **50**, 1405 (2002).
[23] J. Cahn and J. Taylor, Acta Mater. **52**, 4887 (2004).
[24] Z. Shan, E. Stach, J. Wiezorek, J. Knapp, D. Follstaadt, and S. Mao, Science **305**, 654 (2004).
[25] M. Upmanyu, D. Srolovitz, A. Lobkovsky, J. Warren, and W. Carter, Acta Mater. **54**, 1707 (2006).
[26] Z. Trautt and Y. Mishin, Acta Mater. **60**, 2407 (2012).
[27] K.-A. Wu and P. Voorhees, Acta Mater. **60**, 407 (2012).
[28] V. Heinonen, C. V. Achim, K. R. Elder, S. Buyukdagli, and T. Ala-Nissila, Phys. Rev. E **89**, 032411 (2014).
[29] K. R. Elder, M. Katakowski, M. Haataja, and M. Grant, Phys. Rev. Lett. **88**, 245701 (2002).
[30] K. R. Elder and M. Grant, Phys. Rev. E **70**, 051605 (2004).
[31] K. R. Elder, N. Provatas, J. Berry, P. Stefanovic, and M. Grant, Phys. Rev. B **75**, 064107 (2007).
[32] S. van Teeffelen, R. Backofen, A. Voigt, and H. Löwen, Phys. Rev. E **79**, 051404 (2009).
[33] R. Backofen, K. Barmak, K. R. Elder, and A. Voigt, Acta Mater. **64**, 72 (2014).
[34] H. Emmerich, H. Lowen, R. Wittkowski, T. Gruhn, G. I. Tth, G. Tegze, and L. Granasy, Adv. Phys. **61**, 665 (2012).
[35] N. Faghihi, N. Provatas, K. R. Elder, M. Grant, and M. Karttunen, Phys. Rev. E **88**, 032407 (2013).
[36] M. Seymour, F. Sanches, K. R. Elder, and N. Provatas, Phys. Rev. B **92**, 184109 (2015).
[37] M. Greenwood, N. Provatas, and J. Rottler, Phys. Rev. Lett. **105**, 045702 (2010).
[38] N. Ofori-Opoku, J. Stolle, Z.-F. Huang, and N. Provatas, Phys. Rev. B **88**, 104106 (2013).
[39] D. A. Molodov and P. J. Konijnenberg, Scr. Mater. **54**, 977 (2006).
[40] L. Barrales-Mora, V. Mohles, P. J. Konijnenberg, and D. A. Molodov, Comput. Mater. Sci. **39**, 160 (2007).
[41] S. Rivoirard, JOM **65**, 901 (2013).
[42] R. F. Sekerka, Cryst. Res. Technol. **40**, 291 (2005).
[43] J. Han, S. Thomas, and D. Srolovitz, Prog. Mater. Sci. **98**, 386 (2018).
[44] C. Günster, D. A. Molodov, and G. Gottstein, Scr. Mater. **63**, 300 (2010).
[45] C. Köhler, R. Backofen, and A. Voigt, Phys. Rev. Lett. **116**, 135502 (2016).